



HAL
open science

Quantitative element analysis with an energy dispersive X-ray fluorescence instrument equipped with a highly oriented pyrolytic graphite filter

Tetiana Sokoltsova, Eric Esbelin, Marie-christine Lépy

► To cite this version:

Tetiana Sokoltsova, Eric Esbelin, Marie-christine Lépy. Quantitative element analysis with an energy dispersive X-ray fluorescence instrument equipped with a highly oriented pyrolytic graphite filter. X-Ray Spectrometry, 2021, pp.1. 10.1002/xrs.3251 . cea-03328556

HAL Id: cea-03328556

<https://cea.hal.science/cea-03328556>

Submitted on 30 Aug 2021

HAL is a multi-disciplinary open access archive for the deposit and dissemination of scientific research documents, whether they are published or not. The documents may come from teaching and research institutions in France or abroad, or from public or private research centers.

L'archive ouverte pluridisciplinaire **HAL**, est destinée au dépôt et à la diffusion de documents scientifiques de niveau recherche, publiés ou non, émanant des établissements d'enseignement et de recherche français ou étrangers, des laboratoires publics ou privés.

Quantitative analysis with an energy dispersive X-ray fluorescence instrument equipped with a HOPG filter

Tatiana Sokoltsova¹, Eric Esbelin^{1*}, Marie-Christine Lépy²

¹ CEA, DES, ISEC, DMRC, Univ. Montpellier, Marcoule, France

² Université Paris-Saclay, CEA, LIST, Laboratoire National Henri Becquerel (LNE-LNHB), F-91120 Palaiseau, France

*corresponding author: eric.esbelin@cea.fr

ABSTRACT

We present an energy-dispersive X-ray fluorescence (EDXRF) instrumentation mainly intended for the quantitative analysis of actinides based on their intense L X-ray lines. The experimental setup is equipped with a highly oriented pyrolytic graphite (HOPG) optic as a bandpass filter placed between a sample and a detection system. In such an arrangement, it modifies the spectral distribution of the fluorescence radiation and allows recording of a spectrum in the energy range from 10 keV to 18 keV, while suppressing parts considered to be useless. In order to perform accurate quantitative analysis of the recorded spectra, the classical quantification algorithm based on the fundamental parameters must be adapted to take into account the effect of the HOPG optic on the measured intensities. This requires to determine the transmission function of the HOPG filter and implement it in the algorithm. The validity of this approach is checked in different application examples.

Keywords : X-ray fluorescence, quantitative analysis, fundamental parameters, HOPG optic, ray-tracing

1. INTRODUCTION

ATALANTE (ATelier Alpha et Laboratoires pour ANalyses, Transuraniens et Études de retraitement) is a nuclear facility of the French alternative energies and Atomic Energy Commission (CEA). Located on the Marcoule nuclear site, it is dedicated to research into spent nuclear fuel reprocessing and management of high-level long-lived radioactive wastes. The ATALANTE analysis laboratory focuses particularly on the analysis of actinides. Measurements are conducted in glove boxes and in hot cells on samples with radionuclides of intermediate and high levels of radioactivity, respectively. An energy dispersive X-ray fluorescence (EDXRF) system was designed and installed in the hot cell of the laboratory for the explicit purpose of performing analyses of samples containing mainly uranium (U) and plutonium (Pu) based on their intense L X-ray lines [1], [2]. The system includes: i) an Rh-anode X-ray tube (4 kW), ii) a cylindrical highly oriented pyrolytic graphite (HOPG) optic, and iii) a high purity germanium (HPGe) detector. HOPG is a mosaic crystal which consists of a large number of small crystallites and owns a high integrated reflectivity due to a large mosaicity [3], [4], [5]. It is widely used as focusing and dispersion device [6], [7]. In the present experimental ("nuclearized") setup, the HOPG optic is employed as a bandpass filter between the sample and the detector for specific detection of the fluorescence radiation covering the energy range from 12 keV to 17 keV. The X-rays which are outside of the energy range of interest (e.g., characteristic lines of shielding elements and scattered X-ray tube radiation) are thus suppressed that reduces the emission rate [6]. This is especially advantageous for the detection of small contents of

analytes which requires to increase the tube current to get results within a short period of time (typically 800 s). In the present setup, the optic element allows selecting the energy region of L X-ray lines of actinides such as Th, U, Np, Pu, Am, Cm, but also of K lines of Rb, Pb, Sr, Y, Zr. The system is lead-shielded, since the measurements are carried out on high-activity samples, inducing very high dose rates.

The X-ray spectra obtained with the nuclearized setup are quantified with a processing software developed in the laboratory [2] which includes a library of standard spectra. Calibration is performed for each standard element, establishing a nonlinear relationship between the peak intensity and the element concentration [8]. However, the calibration is time-consuming and has to be performed regularly in order to ensure its validity.

A spectrum measured with a conventional EDXRF setup can also be processed using an algorithm based on the fundamental parameters (FP) method [7], [9]. This requires the knowledge of the geometry of the experimental setup, flux and spectral distribution of the excitation radiation, sample matrix, detection efficiency, etc. However, the spectra obtained on the nuclearized setup cannot be quantified in the same manner because the modification of the fluorescence intensities by the HOPG optic is not taken into account in the algorithm. Thus, it is necessary to develop a specific algorithm for the quantitative analysis without standards. This requires to characterize the HOPG response in order to establish a better understanding of its diffraction behavior and define the transmission function. To determine an exact influence of the HOPG filter on the spectral distribution, ray-tracing simulations can be carried out. For the calculations, the exact geometrical parameters of the experimental setup are necessary. Unfortunately, some parameters are not known and the setup cannot be disassembled for such studies for an indefinite period. Thus, this motivated the construction of a miniaturized copy of the nuclearized setup to develop such a FP-based quantification approach and be able to perform tests to get experimental validation.

This article aims to discuss the main characteristics of the miniaturized XRF setup equipped with a HOPG optic. The instrument covers the energy range from 10 keV to 18 keV. During this work, the setup was tested in a non-nuclear laboratory using samples with medium-Z elements (Se, Rb, Sr, Y, etc.) whose K X-ray emission lines are in the same energy range as the actinide L X-ray emission lines. A large part of this paper is devoted to the presentation of the optical model which mimics the detection line (from the sample to the detector) of the miniaturized setup using a ray-tracing algorithm. This is applied to calculate the HOPG transmission function which is included in the FP algorithm enabling an accurate quantification. Selected examples are presented to validate this approach.

2. EXPERIMENTAL SETUP

The studied XRF setup is custom-built and can be considered as a miniaturised copy of the nuclearized system. The principal components of the setup are i) an Ag-anode X-ray tube with a power of 4 W, ii) a HOPG cylinder (Optigraph, Germany) and ii) a silicon drift detector (SDD) (Amptek, USA). The picture of the experimental setup is shown in Figure 1.

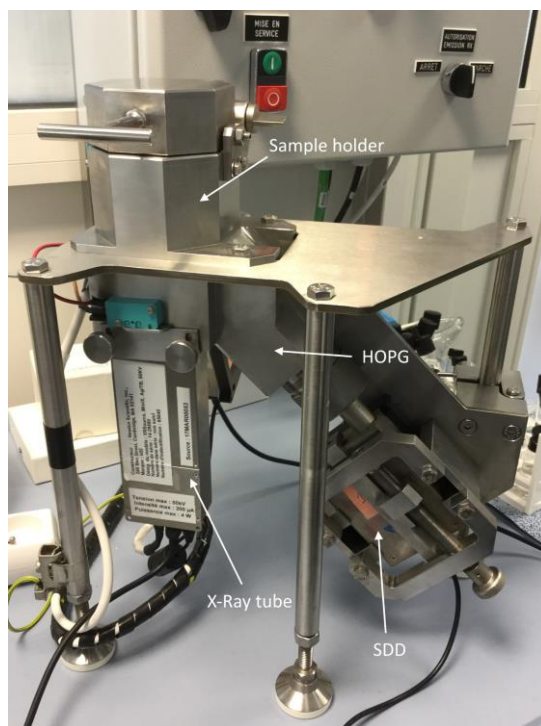


FIGURE 1 Picture of the miniaturized XRF setup

Transmission-anode X-ray tube with a maximum power of 4 W is used to irradiate the sample. The instrument is positioned at an angle of 22° to the normal of the sample holder at a distance of 16 mm from it. The Bragg diffracted fluorescence radiation is focused by the HOPG optic onto the SDD. The SDD is placed on the axis of HOPG cylinder, which is in the plane perpendicular to that of the X-ray tube and tilted at an angle of 46° with respect to the sample holder axis (see Figure 2). The detection line is based on the von Hamos full-cylinder geometry [10] where the sample is regarded as a geometrical source.

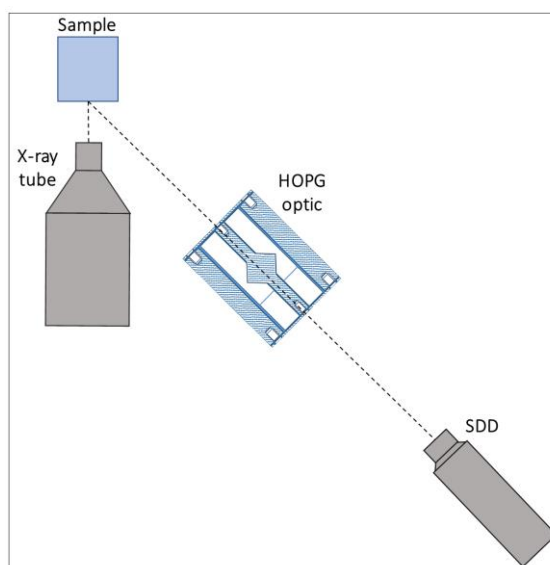


FIGURE 2 Schematic drawing of the experimental setup

To provide radiation shielding, part of the instrument is enclosed in a stainless-steel housing, with a

3 mm thick aluminium (Al) insert to minimize the contribution of fluorescence radiation from the stainless-steel elements. Both the HOPG filter and the silicon detector can be moved separately along their common axis. The samples are placed in a sample cup, which in turn is positioned in an aluminium sample holder. During this work, all samples were prepared from certified standards ($1\ 000\ \text{mg L}^{-1}$ in 2 %HNO₃).

The HOPG optic is a key element of the experimental setup. It has an inner radius R of 10 mm and a length L is 40 mm. The inner surface of the cylinder is coated with a 200 μm thick HOPG layer with a mosaicity of 0.4° (see Figure 3).

The HOPG element was provided with an internal beam stop to avoid the direct transmission of the fluorescence radiation from the sample to the detector without being diffracted [11], [12]. The beam stop is covered with a thin HOPG layer as well.

The energy band reflected by the HOPG optic depends on the size of the geometrical source viewed by the HOPG, the length of the cylinder, the sample-to-HOPG and HOPG-to-detector distances and the detection area. With the experimental setup, the fluorescence radiation is collected in the energy range from 10 keV and 18 keV.

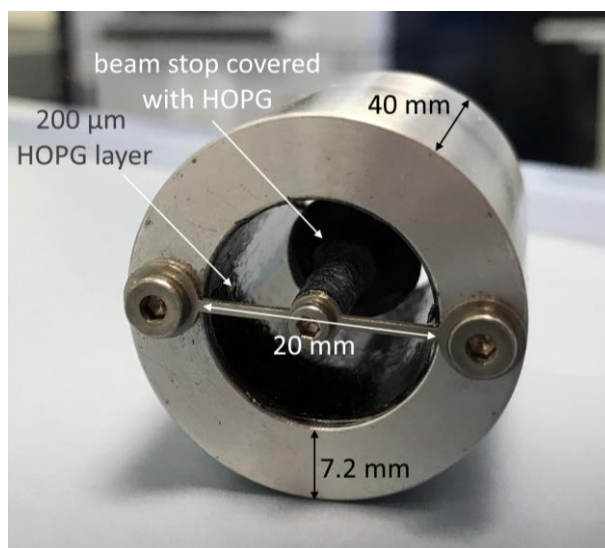


FIGURE 3 HOPG optic

A series of measurement were performed in order to investigate the performances the HOPG filter and demonstrate how this optical element modifies the spectral distribution. Indeed, the HOPG optic can be easily removed to enable recording of the direct X-ray spectrum in the energy range from 3 keV to 30 keV.

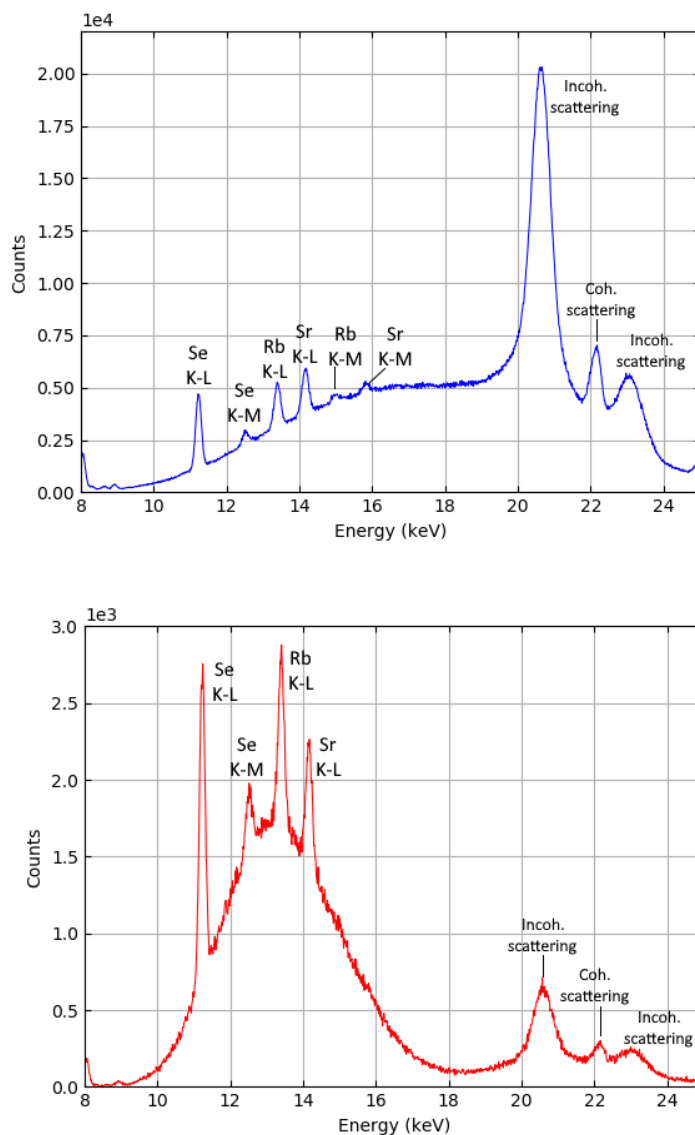


FIGURE 4 Fluorescence spectra of a sample containing Se, Rb and Sr at concentrations of 100, 50 and 50 mg L⁻¹, respectively in HNO₃ 0.5 M measured without (upper panel) and with (lower panel) HOPG optic

As an example, fluorescence spectra of a sample with Se, Rb and Sr recorded without and with HOPG are compared in Figure 4. With the HOPG, the spectrum in the energy band covered by the filter is intense whereas a low-energy part of the spectrum as well as the coherently and incoherently scattered excitation radiation are considerably reduced.

3. QUANTIFICATION ALGORITHM

For the quantification of the spectra recorded without HOPG optic, we used the FP-based software PyMCA developed at the European Synchrotron Research Facility (ESRF) [13]. This uses spectrum evaluation presented by Van Espen and Janssens [14]. In fact, the fluorescence lines of an element can be grouped (e.g. K_{α} , K_{β} groups, or the entire family of lines (K, L, M etc.) of a given element), and characterised by the total number of counts of all lines, A , in a relevant group. The spectrum of an entire element can be expressed as:

$$y_p(i) = A \sum_{j=1}^{N_p} R_j G(i, E_j) \quad (1)$$

where G is the function for a line of energy E_j with relative intensity R_j . N_p represents all the lines in a respective group. The modelling of an entire element permits a reduction in the number of fitting parameters. In the present work, the characteristic X-ray peaks were approximated by a Gaussian function. Other functions such as Lorentzian and Hypermet can also be used to fit the various peaks. The relative transition probabilities of the fluorescence lines between (sub)shells are constant. However, their apparent intensities depend on the absorption in the sample and on absorbers between the sample surface and the active area of the detector. Thus, the attenuation of X-ray must be considered in Eq. (1) to define the correct fitting function. In such a case, the apparent intensities are multiplied by the transition probabilities with an absorption correction term.

In the case of a polychromatic excitation (e.g., the X-ray tube excitation), the approach considers an incident beam of X-rays of energies E_{0k} with relative rates w_k . The relative intensity ratios are defined as:

$$R'_j = \sum_k \frac{w_k T_A(E_{0k}) \omega_j P_j(E_{0k}) R_j T_A(E_j) [1 - T_D(E_j)]}{\mu_T(E_{0k}) + \mu_T(E_j) \frac{\sin \varphi_1}{\sin \varphi_2}} \times \left[1 - \exp \left\{ \left[\frac{\mu_T(E_{0k})}{\sin \varphi_1} \right] + \left[\frac{\mu_T(E_j)}{\sin \varphi_2} \right] \rho d \right\} \right] \quad (2)$$

where ω_j is the fluorescence yield of the given shell, P_j considers the possibility of leaving a vacancy in the j shell, μ_T is the total mass attenuation coefficient of the sample for the primary radiation E_{0k} and the fluorescence radiation E_j , φ_1 and φ_2 are the incoming and outgoing angles of the beam with respect to the sample surface, ρ is the sample density, and d is the sample thickness. The absorption correction terms $T_A(E_{0k})$ and $T_A(E_j)$ consider all attenuators between the sample and the active area of the detector for incident and fluorescence energies, respectively. The second absorption correction term $[1 - T_D(E_j)]$ represents the absorption of the detector for X-rays.

In Eq. (2), this apparent transition has to be taken into account with $R'_j = R_j / \sum_j R'_j$.

The total count rate A in an X-ray group of an element is determined by the incident beam intensity I_0 , the mass fraction C of this element in the sample, and the geometrical efficiency of the detector. The count rate for the group of an element is expressed as:

$$A = I_0 C \frac{\Omega}{4\pi} \sum_j R'_j \quad (3)$$

where Ω is the solid angle of detection, which is determined by the sample-to-detector distance and the sensitive area of the detector.

In Eq.(3), the total count rate A is a measured value. The flux of the excitation radiation can be determined from the reference material and the geometrical efficiency of the detector can be calculated within the software since all setup parameters are known. In the present experimental setup, in addition, the measured fluorescence intensities are also dependent on the transmission of X-

rays through the HOPG optic. Thus, this must be included in Eq. (3) as an extra transmission factor.

4. TRANSMISSION FUNCTION OF THE HOPG FILTER

The investigation of the reflection properties of the HOPG element was performed with the help of the ray-tracing package XRT [15]. The developed optical model includes a source of rays, a HOPG cylinder and an image plane. The sample, being exposed to the primary X-rays, is regarded as the physical source of rays in the simulation model. For the sake of simplicity, the source was modelled as a disc perpendicular to the principal axis of the optical system and parallel to the image plane (see Figure 5). The aperture between the source and the HOPG optical element was created according to the mechanical constructions of the setup which limits the propagation of rays.

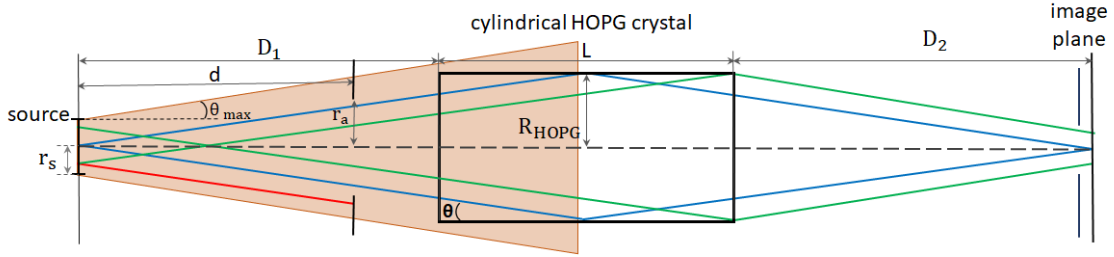


FIGURE 5 Illustration of the ray path from the extended source of radius r_s toward the HOPG cylinder passing the circular aperture of radius r_a

The monoenergetic rays, emitted in a conic ring from a point source lying on the cylinder axis, are reflected from a small crystal surface (blue lines in Figure 5). In the case of an extended source r_s , monoenergetic rays can be emitted from any point of the source and consequently with different directions they impinge on the crystal surface at the same axial position. In this case, the angular acceptance of the optical surface is dependent on the size of the source viewed by the crystal, the size of the crystal, and its distance from the source D_1 . Thus, all effective angles need to be considered in this respect.

Rays are incident on the optical surface with an angle θ lying in the range:

$$\arctan\left(\frac{R - \Delta r_s}{D_1 + L}\right) \leq \theta \leq \arctan\left(\frac{R + \Delta r_s}{D_1}\right) \quad (4)$$

The effective incident angles dictated by Eq. (4) are further limited by the circular aperture of a radius r_a at a distance d from the source. Thus, the condition (4) must satisfy the next relation:

$$\arctan\left(\frac{r_a - \Delta r_s}{d}\right) \leq \theta \leq \arctan\left(\frac{r_a + \Delta r_s}{d}\right) \quad (5)$$

From Eq. (4) and Eq. (5), the maximum θ_{max} angle can be calculated to define the angle of the truncated cone delimiting the beam source (see Figure 5, red shaded area). Thus, all possible angles on the crystal surface are taken into account.

Since rays from an extended source propagate with a uniform distribution and with all their directions from the starting point to the optical surface, it is necessary to include a beam stop to prevent direct passing of rays. The exact shape of the beam stop is complicated to reproduce in the simulation model. It can be represented as simple obstacles in the system: two identical circular beam stops on each side of the cylinder and a larger one in the centre, as depicted in Figure 6. The energy window of the

collected X-rays is dependent on the solid angle of detection subtended by the detector from the HOPG cylinder, i.e., the detector size and crystal-to-detector distance D_2 . In order to model the detection area of the SDD, a circular aperture of a size equivalent to that of Si was positioned just in front of the image plane. Thus, the beam collected on the image plane is representative of the detector view.

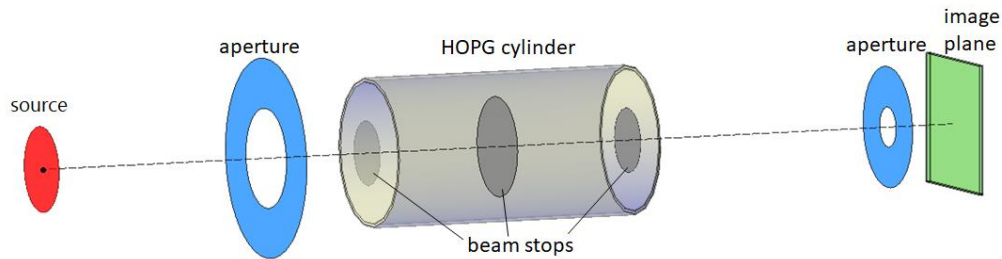


FIGURE 6 Illustration of the complex optical system for ray-tracing simulation, including all principal components

Let us define the central energy as the energy of the rays reflected from the centre of the HOPG cylinder in the case of a point source (see Figure 5, blue lines). In the geometrical configuration with equal distances D_1 and D_2 , the reflectivity from the first and second order reflections can be calculated. For example, in the case of a point source and a mosaic crystal [16] to maximize the first order of reflection of 13 keV rays the distances D_1 and D_2 must be set at 50 mm. In this arrangement, the rays of twice the central energy are reflected in the second order. These rays with higher energies can be reflected from deeper crystal planes, contributing to the output results. Since the experimental measurements were performed at up to over 30 keV, both the first and second orders of reflection had to be computed.

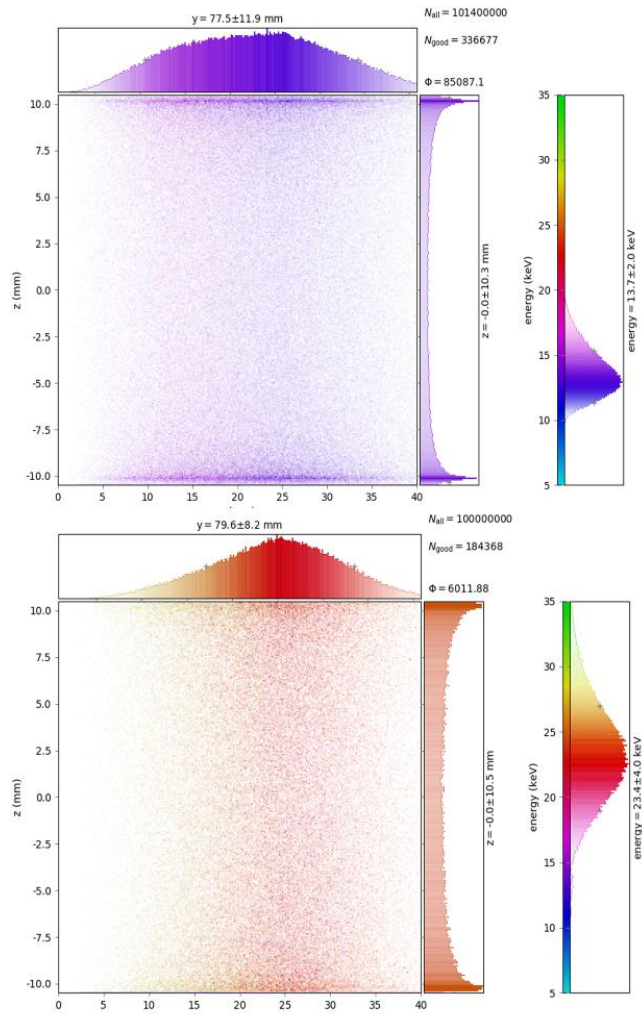


FIGURE 7 Simulation of the reflectivity for the polychromatic beam in the energy range from 5 keV to 35 keV in the first (upper panel) and second (lower panel) orders of reflection. Both simulations were performed for the central energy of 13 keV in the first order of reflection

From Figure 7, it can be seen that rays reflected in the first order of reflection are collected in the energy range from 10 keV to 17 keV, while the rays with energies from 15 keV to 33 keV correspond to the second order of reflection. It is important to point out that almost all optical surface contributes to the first order of reflection, whereas only a narrower part of the crystal reflects the rays in the second order. The full width at half maximum (FWHM) of profiles are 4 keV and 8 keV in the first and second order of reflections, respectively.

The intensities of the reflected rays in the second order are much lower, however, and they appear in the energy range of the coherent and incoherent scattering of the excitation radiation. The calculations were performed separately for the same number of rays.

The reflection profile of the optical element with the source sampled with a uniform ray distribution was first calculated. At this point, it is necessary to represent mathematically the output of ray distribution after the crystal, in order to integrate it into the PyMCA code. However, since the broadening of the reflection profile varies with the HOPG filter position, the response had to be calculated for each desirable central energy.

The reflection profiles of the HOPG optic in the first and second orders of reflection are asymmetric. The complex profile could be fitted with several Gaussian functions [17], but this would involve a

large number of parameters. To simplify the fitting of the filter output and perform it independently of the cylinder position, a spline function was used. This estimates a spline representation of the curve and can be evaluated for a desired set of points. Figure 8 illustrates the complex reflection profile calculated with XRT (blue line) and fitted by spline function (red line).

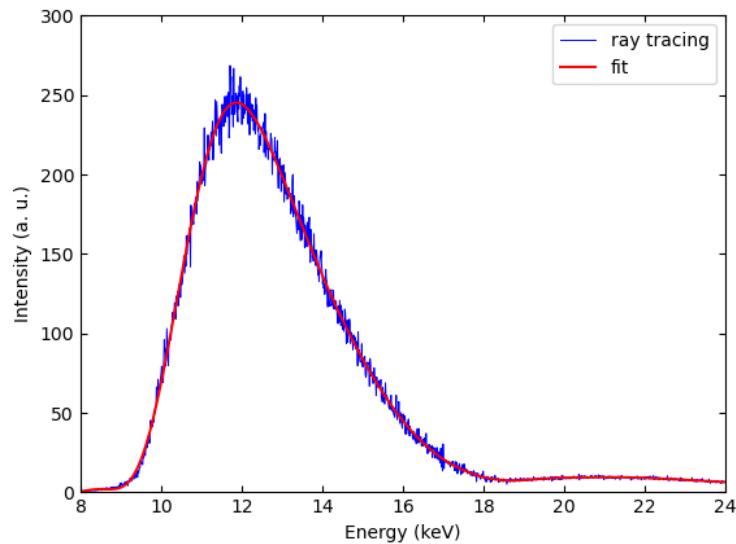


FIGURE 8 Fit of the reflection profile of the HOPG filter calculated with the source sampled with a uniform ray distribution by means of the ray-tracing method. Calculations were performed in the first and second orders of reflection

5. RESULTS AND DISCUSSION

Without considering of the transmission function of the HOPG optic, a spectrum is processed incorrectly by the PyMCA package. In Figure 9, it can be seen that the Sr peaks are fitted inaccurately, especially the Sr K-M peak which is largely overestimated by the software. The latter peak is located on the shoulder of the hump of the spectrum, where the transmission is reduced.

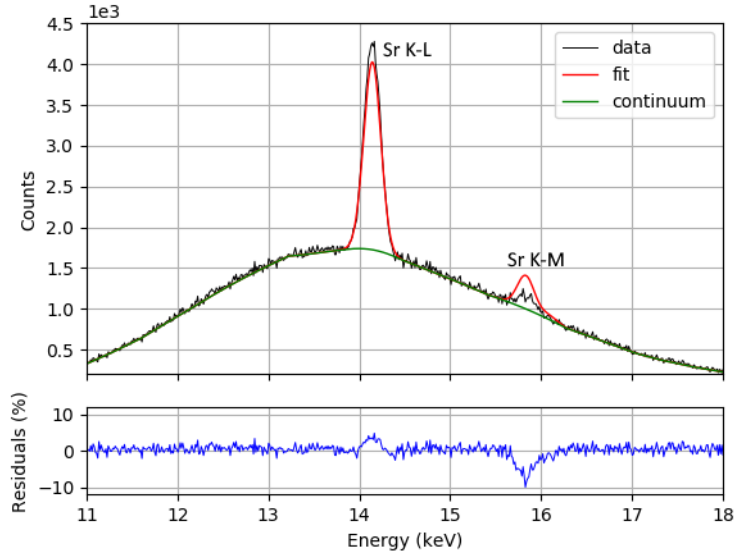


FIGURE 9 Processing of the spectrum from the sample with 100 mg L^{-1} of Sr in HNO_3 0.5 M. The spectrum analysis model does not take into account the modification of spectral distribution by the HOPG filter

In fact, the model can consider the presence of the bandpass filter as a new attenuator between the sample and the detector. To take this into account in Eq. (3), each relative intensity R'_j of the line of energy E_j is multiplied by a new attenuator term T_{M_j} , which is the relevant transmission function estimated for given positions of the HOPG cylinder and the SDD.

Thus, the apparent intensities become:

$$R_j^* = [R'_j * T_{M_j}] \quad (6)$$

This approach was implemented in the PyMca code.

In order to validate the new spectrum analysis model, several experiments were performed with different samples and at various distances D_1 and D_2 . A number of transmission functions for central energies in the range from 12.8 keV to 15 keV were calculated beforehand, to be applied in the model. Figure 10 shows the spectrum acquired for the solution containing 100 mg L^{-1} of Se in HNO_3 0.5 M (black line) and the result of the fit (red line). The comparisons of the prepared and estimated mass fractions are reported in Table 1 (Processing №1).

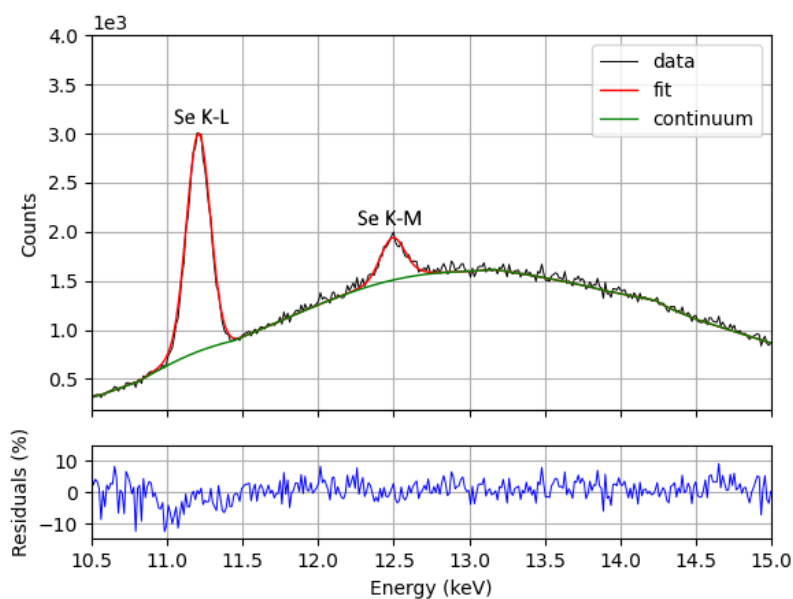


FIGURE 10 Processing of the spectrum from the sample containing Se at a concentration of 100 mg L^{-1} in HNO_3 0.5 M

Another example of a fit procedure is depicted in Figure 11. For this experiment, Rb and Y at a concentration of 100 mg L^{-1} of each element in HNO_3 0.5 M were used. The HOPG cylinder was positioned at the furthest possible distance from the sample surface allowed by the setup to reach the central energy of 15 keV. It can be seen that the fitting of the spectrum has been performed accurately, and that the Y K-L and Rb K-M peaks are resolved. Thus, only small deviations of the computed concentrations from the prepared values are observed (see Table 1, Processing №2).

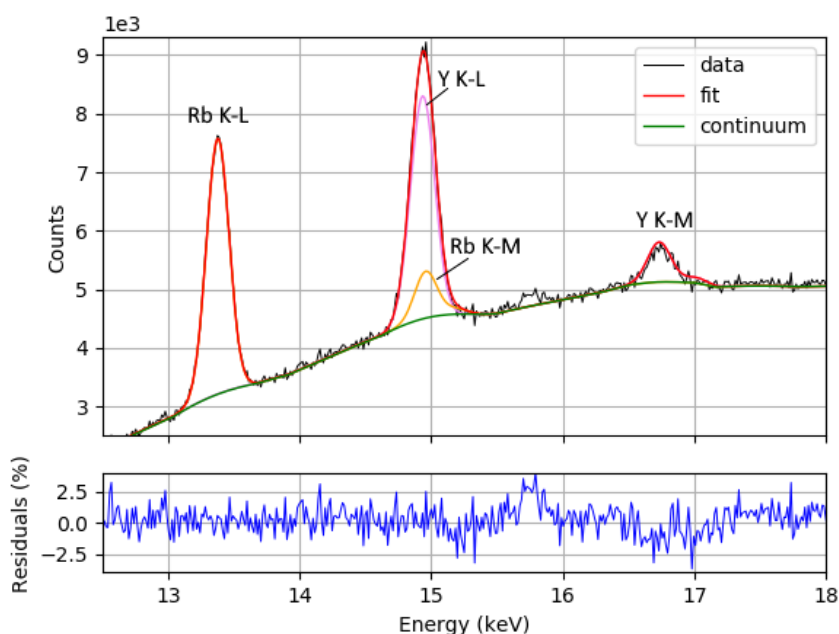


FIGURE 11 Processing of the spectrum from the sample containing Rb and Y at concentrations of 100 mg L^{-1} in HNO_3 0.5 M

To go further in the analyses, the spectrum from a sample with three elements at different

concentrations was processed (see Figure 12). It can be seen that the lines on the shoulders of the hump, where the reflectivity is decreased, fit perfectly. The concentrations of all elements in the sample could be accurately calculated, despite intensities reduced by the filter (see Table 1, Processing №3).

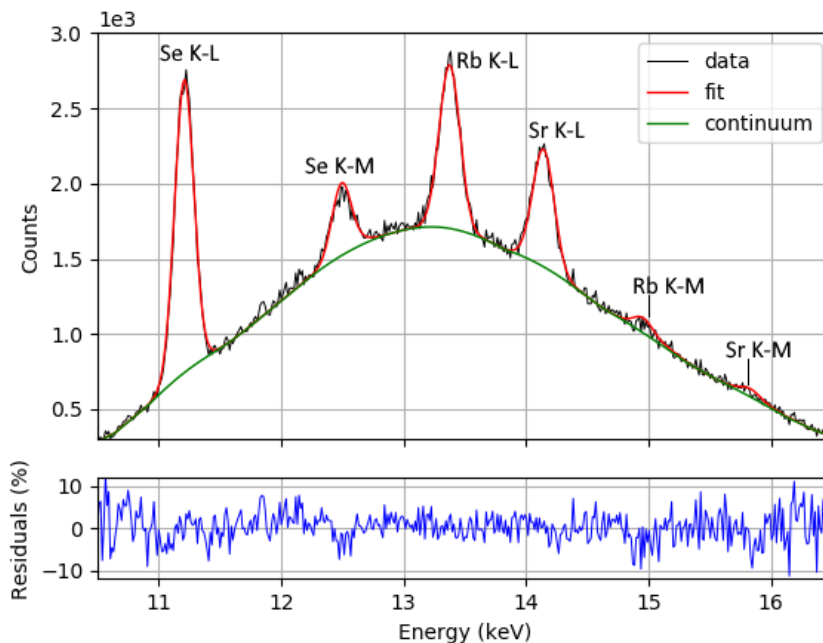


FIGURE 12 Processing of the spectrum from a sample with 100, 50, and 50 mg L⁻¹ of Se, Rb, and Sr, respectively, in HNO₃ 0.5 M

6. CONCLUSIONS

We demonstrated the possibility of analysing spectra obtained with an EDXRF setup equipped with HOPG optic, using a quantification algorithm based on the fundamental parameters. The HOPG optic device was used as a broadband filter, which favoured the collection of the fluorescence radiation in the desired energy ranges, and suppressed the low energy peaks and scattered radiation of the excitation source. The selected energy domain extended from 10 keV to 18 keV, which corresponds to that of the actinide L X-ray lines.

For the accurate quantitative analysis of the recorded spectra, the transmission function of the HOPG cylinder (taken into account both the first and second orders of reflexion) was calculated by means of the ray-tracing package XRT. This enabled us to represent the entire detection channel of the experimental setup. The calculated transmission functions, fitted with spline functions, were implemented in the FP-based code PyMCA in such a way that each intensity of each measured line of a given energy was multiplied by the relevant transition efficiency. The new model was tested for different concentrations of medium-Z elements (Se, Rb, Sr, Y). While the direct quantification, i.e. without the calculation of HOPG transmission, was strongly biased with relative differences up to 50 % compared to the prepared mass fractions. Whereas, the new approach successfully estimated mass fractions with a relative difference less than 5 % from the prepared values. More details on this work can be found in the exhaustive study [18]. In the future, this approach could be applied to the

nuclearized instrumentation in order to avoid time-consuming calibration steps.

ACKNOWLEDGEMENTS

We are grateful to Konstantin Klementiev from MAX IV Laboratory (Lund, Sweden) for his help and valuable advices. We acknowledge also the team of Prof. Birgit Kanngießer from the Berlin Laboratory for innovative X-ray technologies (BLIX) and notably Richard Gnewkow for fruitful discussions on the application of HOPG optics.

References

- [1] E. Esbelin, *AIEA Symposium on International Safeguards: Linking Strategy, Implementation and People*. **2014**.
- [2] E. Esbelin, *X-Ray Spectrom.* **2014**; 43, 198.
- [3] I. G. Grigorieva, A. A. Antonov, *X-Ray Spectrom.* **2003**; 32, 64.
- [4] H. Legall, H. Stiel, V. Arkadiev, A. A. Bjeoumikhov, *Opt. Express*. **2006**; 14, 4570.
- [5] H. Legall, H. Stiel, V. Arkadiev, *Proceedings of FEL*, 798 **2006**;
- [6] Y. Kolmogorov, V. Trounova, *X-Ray Spectrom.* **2002**; 31, 432.
- [7] B. Beckhoff, B. Kanngießer, N. Langhoff, R. Wedell, H. Wolff (Eds.). *Handbook of Practical X-Ray Fluorescence Analysis*. Springer, **2006**.
- [8] R. M. Rousseau, *Spectrochim. Acta - Part B*, **2006**; 61, 759.
- [9] S. K Sharma, in *X-Ray Spectroscopy*. (Eds: R. Sitko, B. Zawisz), InTech, **2012**, pp. 137-162
- [10] L. Anklamm, C. Schlesiger, W. Malzer, D. Grötzsch, M. Neitzel, B. Kanngießer, *Rev. Sci. Instrum.* **2014**; 85, 053110.
- [11] A. A. Antonov, V. B. Baryshev, I. G. Grigoryeva, G. N. Kulipanov, Y. V Terekhov, N. N. Shipkov, *Rev. Sci. Instrum.* **1989**; 60, 2462.
- [12] A. A. Antonov, V. B. Baryshev, I. G. Grigoryeva, G. N. Kulipanov, N. N. Shchipkov, *Nucl. Inst. Methods Phys. Res. A*, **1991**; 308, 442.
- [13] V. A. Solé, E. Papillon, M. Cotte, P. Walter, J. Susini, *Spectrochim. Acta - Part B*, **2007**; 62, 63.
- [14] R. E. Van Grieken, A. A. Markowicz. *Handbook of X-ray Spectrometry Second edition*. Marcel Dekker, Inc., **2001**.
- [15] K. Klementiev, R. Chernikov, *Proc. of SPIE Vol. 9209 92090A-1*, **2014**.
- [16] M. Sanchez del Rio, M. Gambaccini, *Proc. SPIE*, 246, **1998**.
- [17] T. S. Matthew Newville, et al, **Release Notes**, **2018**.
- [18] T. Sokoltsova, PhD thesis, Université Paris-Saclay, **2021**.

TABLE 1 Comparison of prepared and estimated mass fractions with PyMCA, taking into account the transmission function of the HOPG filter

Processing	Element	Prepared mass fraction	Estimated mass fraction	Relative difference, %
1	Se	9.79×10^{-5}	10.25×10^{-5}	+5 %
2	Rb	9.79×10^{-5}	10.22×10^{-5}	+4 %
	Y	9.79×10^{-5}	9.24×10^{-5}	-5 %
3	Se	9.79×10^{-5}	9.58×10^{-5}	-2 %
	Rb	4.89×10^{-5}	4.80×10^{-5}	+2 %
	Sr	4.89×10^{-5}	4.92×10^{-5}	+0.6 %